Tetrahedral Onsager Crosses for Solubility Improvement and Crystallization Bypass

Isabelle Aujard,[†] Jean-Pierre Baltaze,[‡] Jean-Bernard Baudin,[†] Emmanuelle Cogné,[†] Fabien Ferrage,[‡] Ludovic Jullien,*[,†] Éric Perez,[§] Valéry Prévost,[†] Lin Mao Qian,[§] and Odile Ruel[†]

Contribution from the Department of Chemistry and the Department of Physics, École Normale Supérieure, 24, rue Lhomond, F-75231 Paris Cedex 05, France

Received January 2, 2001

Abstract: Pure organic molecules exhibiting a suitable concave rigid shape are expected to give porous glasses in the solid state. Such a feature opens new opportunities to avoid crystallization and to improve molecular solubility in relation to the high internal energy of these solid phases. To quantitatively explore the latter strategy, a series of rigid tetrahedral conjugated molecules ***n*C** and the corresponding models ***n*R** have been synthesized. Related to the present purpose, several properties have been investigated using UV absorption, steady-state fluorescence emission, differential scanning calorimetry, ^{1}H NMR translational self-diffusion, magic angle spinning ^{13}C NMR, and multiple-beam interferometry experiments. The present tetrahedral crosses are up to 8 orders of magnitude more soluble than the corresponding model compounds after normalization to the same molecular length. In addition, they give concentrated monomeric solutions that can be used to cover surfaces with homogeneous films whose thickness goes down to the nanometer range. Such attractive features make cross-like molecular architectures promising for many applications.

Introduction

Chemists from different fields often face problems for solubilizing organic molecules or for avoiding their crystallization. In synthesis, poor solubility constrains to use large amounts of solvent. In addition such a feature may prevent the application of efficient purification procedures such as column chromatography, for instance. For drug applications, solubility is also an essential aspect for access to biological targets. To obtain amorphous films free from inclusion of solid particles or aggregates for optical uses, the manufacturing of organic layers by solution processing requires avoiding phase separation during solvent evaporation. Hence, many approaches have been empirically developed to improve solubility at the molecular level.[1,2] Nevertheless, the diversity of situations encountered by chemists makes always desirable the design of new strategies for favoring dissolution of solid organic phases.

Most existing approaches belong to two different categories that are more easily analyzed in reference to a process leading to the dissolution of a molecular compound M such as:

$$M(s) = M(s) \qquad (1)$$

where M(s) and M(*s*) respectively stand for M in solid phase and in solution. For the convenience of the subsequent analysis,

one may formally decompose the latter process in two steps, sublimation and solvation, involving M(g) in the gas phase:

$$M(s) = M(g) \qquad (2)$$
$$M(g) = M(s) \qquad (3)$$

In the first class of approaches to promote dissolution, the standard[3] Gibbs free energy of dissolution $\Delta_1 G°(T) = \Delta_1 H°(T) - T\Delta_1 S°(T)$ is dominated by the enthalpic term.[4] An appropriate solvent exhibiting a polarizability rather similar to that of the solute is first chosen to avoid phase separation between the solute and the solvent (the first aspect of the rule-of-thumb "like dissolves like").[5] Even in such a case, the dissolution enthalpy $\Delta_1 H°(T)$ is expected to remain positive in the absence of specific interactions. In fact, a solid phase of an organic compound is more compact than the corresponding liquid phase; thus, stabilizing van der Waals interactions are expected to be stronger in the solid phase ($\Delta_2 H°(T) > -\Delta_3 H°(T) \leftrightarrow \Delta_1 H°(T) > 0$). Hence dissolution is generally determined along this strategy by introducing specific groups devoted to strongly interact with the solvent (charged groups in polar solvents or hydrogen bonds in protic solvents, for instance; the second aspect of the rule-of-thumb, "like dissolves like"). Such an approach gives rise to a large negative contribution to the standard solvation

† Département de Chimie (CNRS UMR 8640), Ecole Normale Supérieure, 24, rue Lhomond, F-75231 Paris cedex 05 (France). Fax: (+33) 1 44 32 33 25. E-mail: Ludovic.Jullien@ens.fr.

‡ Département de Chimie (CNRS UMR 8642), Ecole Normale Supérieure, 24, rue Lhomond, F-75231 Paris cedex 05 (France).

§ Département de Physique (CNRS UMR 8550), Ecole Normale Supérieure, 24, rue Lhomond, F-75231 Paris cedex 05 (France).

(1) *Techniques of Organic Chemistry*; Weissberger, A., Ed.; *Separation and Purification*; Interscience Publishers: New York, 1956; Vol. III, Part I, p 549.

(2) *Vogel's Textbook of Practical Organic Chemistry*, 4th ed; Longman: London and New York, 1978.

(3) As commonly encountered, standard states are defined in the text as (i) the pure solid in the solid phase; (ii) the ideal gas at 1 bar in the gas phase; (iii) the ideal solute at 1 M for the diluted solution at *T*.

(4) In the following, the subscripts to the operator Δ refer to the considered process: (1) for dissolution, (2) for sublimation, and (3) for solvation.

(5) (a) Hildebrand, J. H.; Prausnitz, J. M.; Scott, R. L. *Regular and Related Solutions*; Van Nostrand Reinhold: Princeton, 1970. (b) Reichardt, C. *Solvent and Solvent Effects in Organic Chemistry*, 2nd ed; VCH: Weinheim, Basel, Cambridge, New York, 1988. (c) Israelachvili, J. N. *Intermolecular and Surface Forces*, 2nd ed; Academic Press: London, San Diego, New York, Boston, Sydney, Tokyo, Toronto, 1992.
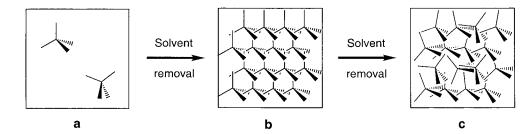
Figure 1. Schematic picture illustrating the phenomena expected to occur during the evaporation of a solution of tetrahedral Onsager crosses under quasistatic conditions. (a) diluted solution, isolated crosses; (b) above a critical concentration *C**; (c) without solvent, disordered porous solid phase.

enthalpy $\Delta_3 H°(T)$ that is expected to counterbalance the above-mentioned density effect. In the second category of approaches to promote dissolution, enthalpy plays a minor role, and entropy dominates the Gibbs free energy of dissolution. The strategy is based on introducing molecular degrees of freedom that are frozen in the solid state but active in solution.[6] This is most conveniently achieved by playing with internal rotations. Thus, flexible substituents such as alkyl, polyoxyethylenic, or siloxane chains are often grafted to a solute to improve its solubility. Hence, most dissolution strategies rely on the features of the solute M(*s*). Nevertheless, consideration of the processes 1, 2, and 3 shows that the Gibbs free energy of dissolution of an organic compound is governed by its chemical potential in both phases: solid and solution. Thus, one can also destabilize the solid phase to improve solubility. Then the reasoning exposed above suggests that decreasing the density of the solid phase could provide an efficient way to increase the standard enthalpy of the solid phase so as to decrease the standard Gibbs free energy of dissolution. A possible approach to obtain poorly compact solid phases consists of designing molecules of suitable shapes.

The present paper is conceived to explore the latter dissolution strategy based on engineering the destabilization of the solid phase of a molecular organic compound. Despite existing publications evoking related facts during the course of diverse studies,[7] this report seems to be the first to quantitatively evaluate such an approach for improving solubility and to draw its limits. Among possible molecular structures for the present purpose, a series of molecules *n*C that can be reasonably considered as Onsager crosses has been selected. Onsager crosses are attractive hard nonconvex bodies formed by rigidly connecting elongated rods that were named as a tribute to Onsager's seminal contributions to the theory of lyotropic crystals.[8] Under quasi-static conditions, solvent evaporation from a diluted solution of isolated Onsager crosses is expected to give (i) a homogeneous ordered network of connected crosses at a critical concentration *C** related to the rod length,[8] (ii) a

porous glass after solvent removal (Figure 1). It is the latter porosity that is anticipated to ultimately drive the solubility increase. In the present manuscript, solubility and differential scanning calorimetry experiments have been performed to quantitatively analyze the solubility of the *n*C molecules. In light of the behavior of the model compounds *n*R, the results are analyzed with a thermodynamic model developed to extract the true significance of the molecular architecture on solubility properties. In addition to the preceding favorable feature for dissolution, the large anisotropy for molecular interaction between Onsager crosses may also keep low enough the solution viscosity during the solvent evaporation up to the critical concentration *C**. Together with solution homogeneity, such a feature could be useful for applications in which a homogeneous coating is expected from the spreading and the evaporation of a solution (spin-coating for instance). Although not yielding a regular lattice, the latter approach to obtain organic nanoporous materials can be also considered as an interesting alternative to engineer a crystal network by design from molecular structure.[9] In fact, the rigidity of Onsager crosses should prevent some drawbacks that are commonly encountered when using noncovalent strategies to build up nanoporous media since crystal collapse usually occurs upon removal of interstitial solvent.[10] In the present paper, we also report on complementary NMR and interferometry experiments aiming to illustrate the latter aspects.

Results

Molecular Design and Synthesis. Many chemical compounds obey the generic structure of Onsager crosses. In fact, several have already been reported in the litterature.[7,11] For the present purpose, we sought for a homologous series of crosses made of rigid rods grafted onto a central node and for the series of corresponding model compounds. Different synthetic methodologies lead to rodlike structures exhibiting a reduced conformational flexibility. Among them, we favored the *p*-phenylyne building strategy via palladium-catalyzed coupling. The latter has been already extensively used in supramolecular chemistry. It is particularly suitable for obtaining a series of molecules of increasing length.[12] Instead of adopting an octahedral node as it has been done in theoretical studies,[8] the tetrahedral tetraphenylmethane core was chosen.[7d,13] In view

(6) See for instance: (a) Hildebrandt, J. H.; Scott, R. L. *The Solubility of Nonelectrolytes*, 3rd ed; Reinhold Publishing Corporation, New York, 1950; (b) Leffler, J. E.; Grunwald, E. *Rates and Equilibria of Organic Reactions as Treated by Statistical, Thermodynamic, and Extrathermodynamic Methods*; Dover: New York, 1963. (c) Benson, S. W. *Thermochemical Kinetics Methods for Estimation of Thermochemical Data and Rate Parameters*, 2nd ed; John Wiley & Sons: New York, London, Sydney, Toronto, 1976.

(7) (a) Wilson, L. M.; A. C. Griffin, *J. Mater. Chem.* **1993**, *3*, 991−994. (b) Mongin, O.; Gossauer, A. *Tetrahedron* **1997**, *53*, 6835−6846. (c) Johansson, N.; Salbeck, J.; Bauer, J.; Weissörtel, F.; Bröms, P.; Andersson, A.; Salaneck, W. R. *Adv. Mat.* **1998**, *10*, 1136−1141 and references therein. (d) Wang, S.; Oldham, W. J., Jr.; Hudack, R. A., Jr.; Bazan, G. C. *J. Am. Chem. Soc.* **2000**, *122*, 5695−5709 and references therein.

(8) (a) Frenkel, D. In *Liquids, Freezing and Glass Transition*; Hansen, J. P., Levesque, D., Zinn-Justin, J., Eds.; Elsevier: North-Holland, Amsterdam, 1991. (b) Blaak, R.; Mulder, B. M. *Mol. Phys.* **1998**, *94*, 401−405. (c) Blaak, R.; Mulder, B. M. *Phys. Rev. E* **1998**, *58*, 5873−5884.
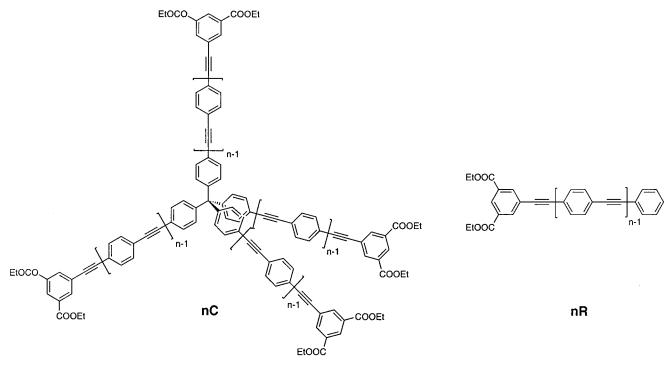
(9) Zaworotko, M. J. *Angew. Chem., Int. Ed.* **2000**, *39*, 3052−3054.
(10) Batten, S. R.; Robson, R. *Angew. Chem., Int. Ed.* **1998**, *37*, 1460−1494.
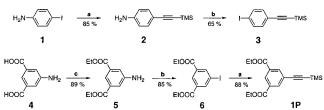(11) Yao, Y.; Tour, J. M. *J. Org. Chem.* **1999**, *64*, 1968−1971.
(12) (a) Tour, J. M. *Acc. Chem. Res.* **2000**, *33*, 791−804. (b) Lavastre, O.; Ollivier, L.; Dixneuf, P. H. *Tetrahedron* **1996**, *52*, 5495−5504. (c) Hsung, R. P.; Chidsey, C. E. D.; Sita, L. R. *Organometallics* **1995**, *14*, 4808−4815.
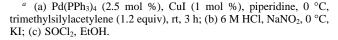(13) (a) Simard, M.; Su, D.; Wuest, J. D. *J. Am. Chem. Soc.* **1991**, *113*, 4696−4698. (b) Su, D.; Menger, F. M. *Tetrahedron Lett.* **1997**, *38*, 1485−1488.

Scheme 1

Scheme 2[a]

[a] (a) Pd(PPh$_3$)$_4$ (2.5 mol %), CuI (1 mol %), piperidine, 0 °C, trimethylsilylacetylene (1.2 equiv), rt, 3 h; (b) 6 M HCl, NaNO$_2$, 0 °C, KI; (c) SOCl$_2$, EtOH.

of previous investigations, the latter can be easily incorporated in synthetic sequences involving palladium coupling. Additional constraints related to purifications and characterizations led to choosing the crosses *n*C and models *n*R (*n* = 1, 2, 3) (pictured in Scheme 1) as targets. 1-Iodo-4-(trimethylsilylethynyl)benzene (**3**) plays a central role in the present synthesis since it is repetitively used for extending the rods (Scheme 2). It was prepared in two steps according to classical procedures.[14] Palladium(0)-mediated coupling of 4-iodoaniline (**1**) with tri-methylsilylacetylene yielded 4-(trimethylsilylethynyl)aniline (**2**) that was subsequently transformed into **3** by iodination of the diazonium salt. The rods were built from the diester terminal ring. The protected alkyne **1P** was easily prepared from 5-(amino)isophthalic acid (**4**) in three steps with good yields (Scheme 2). Esterification of **4** gave diethyl-5-(amino)isoph-thaloate (**5**)[15] that was transformed into diethyl-5-(iodo)-isophthaloate (**6**) by diazotation followed by iodination. Palladium-(0)-mediated coupling of **6** with trimethylsilylacetylene affoarded **1P**. The protected rods (*n*P) were prepared in excellent yields upon repeating an extension sequence: (i) removal of the trimethylsilyl-protecting group in (*n*P) (*n* = 1, 2) by cesium carbonate in ethanol/dichloromethane to give the corresponding

deprotected species (*n*H); (ii) Palladium(0)-mediated coupling of *n*H with **3** to give (*n* + **1**)P (Scheme 3). Eventually, palladium(0)-mediated coupling of the deprotected rods *n*H (*n* = 1, 2, 3) with tetrakis[4-(iodo)phenyl]methane (**8**)[13,16] or with iodobenzene (**9**), respectively, yielded the final crosses *n*C and the corresponding model compounds *n*R (*n* = 1, 2, 3; Schemes 1 and 4). All of the molecules in the *n*R series and **1C** easily gave crystals, whereas **2C** and **3C** were only obtained as solid powders. The final targets were characterized by ^{1}H NMR and ^{13}C NMR, microanalyses, and mass spectrometry. In the case of **2C** and **3C**, ^{1}H NMR and microanalyses revealed the presence of residual solvent despite extensive drying in a high vacuum (See Figure 1S).

Compared Absorption and Steady-State Emission Properties of *n*C and *n*R. UV absorption and fluorescence emission properties have been investigated at room temperature in dichloromethane to subsequently determine the *n*C and *n*R solubilities. Figure 2 and Table 1 summarize the results. All of the species strongly absorb in the 300–350 nm range. Except for the smallest species **1C** and **1R**, *n*C/*n*R absorption bands compare well in the investigated wavelength range. The absorption bands of **2C** and **3C** are only slightly red-shifted with regard to the corresponding band in **2R** and **3R**. After normalization to the same number of chromophores, the molar absorption coefficients at the wavelength of maximal absorption are similar in the *n*C and *n*R series (*n* = 2, 3). In contrast, the observed **1C** absorption band is significantly altered with regard to that of **1R**; **1C** UV absorption is red-shifted and more intense. These results are in agreement with the expected trend based on varying the distance between interacting chromophores.[17] In the present system, the increase of the interchromophoric distance when *n* is increased in the *n*C series is not counterbal-anced by the corresponding increase of the chromophore oscillator strength. Consequently, alterations of the absorption

(14) Takahashi, S.; Kuryama, Y.; Sonogashira, K.; Hagihara, N. *Synthesis* **1980**, 627–630.

(15) Hosangadi, B. D.; Dave, R. H. *Tetrahedron Lett*. **1996**, *37*, 6375–6378.

(16) (a) Merkushev, E. B.; Simakhina, N. D.; Koveshnikova, G. M. *Synthesis* **1980**, 486–487. (b) Neugebauer, F. A.; Fisher, H.; Bernhardt, R. *Chem. Ber*. **1976**, *109*, 2389–2394.

(17) Cantor, C. R.; Schimmel, P. R. *Biophysical Chemistry*; Freeman: New York, 1980; Part II.
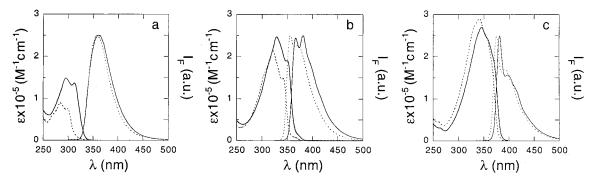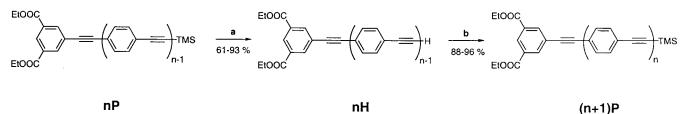
Figure 2. Absorption (thick lines) and emission (thin lines) spectra of *n*R (dotted lines) and *n*C (solid lines) in methylene chloride at 298 K; (a) *n* = 1, (b) *n* = 2, (c) *n* = 3. For a purpose of comparison, molar absorption coefficients have been normalized; thus ϵnC are compared to 4ϵnR. Steady-state emission spectra have been normalized at the wavelength of maximal emission. Excitation wavelength: 260 nm for **1R** and **1C**, 310 nm for the other molecules.

Scheme 3[a]

^{a} (a) Cs_2CO_3 (1.1 equiv), EtOH, CH_2Cl_2; (b) $Pd(PPh_3)_4$ (2 mol %), CuI (1 mol %), **3** (1 equiv), piperidine, rt, 2 h.
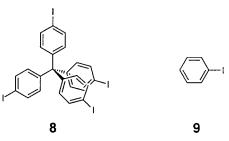
Scheme 4

Table 1. Photophysical Features of the Molecular Rods (*n*R) and Crosses (*n*C) in Methylene Chloride at 298 K (*n* = 1–3)

molecule	$\lambda_{max,abs}$ (nm)^a [ϵ (M^{-1} cm^{-1})]	$\lambda_{max,em}$ (nm)^b [Φ]^c
1R	284 [2.3 × 10^4]	357 [0.15]
2R	322 [5.4 × 10^4]	356 [0.75]
3R	341 [7.3 × 10^4]	375 [0.80]
1C	296 [15 × 10^4]	361 [0.25]
2C	329 [25 × 10^4]	367 [0.75]
3C	346 [27 × 10^4]	381 [0.90]

^{a} Wavelength of maximum absorption in the 250–500 nm range. ^{b} Wavelength of maximum emission in the 300–750 nm range; excitation wavelength: 260 nm for **1R** and **1C**, 310 nm for the other molecules. ^{c} Quantum yield of fluorescence at 298 K.

features are more pronounced for **1C** than for **2C** and for **3C**. *n*C and *n*R molecules are also strongly fluorescent in the 350–500 nm wavelength range. Nevertheless, in contrast to the absorption features, the steady-state emission spectra of *n*R and *n*C are not significantly different.[18]

Compared Solubilities of *n*C and *n*R. As anticipated, the crosses *n*C are soluble in most organic solvents used in the

(18) Bazan, Mukamel, and co-workers recently investigated the photophysical properties of a series of compounds related to the present molecules (Bazan, G. C.; Oldham, W. J., Jr.; Lachicotte, R. J.; Tretiak, S.; Chernyak, V.; Mukamel, S. *J. Am. Chem. Soc.* **1998**, *120*, 9188−9204; Wang, S.; Bazan, G. C.; Tretiak, S.; Mukamel, S. *J. Am. Chem. Soc.* **2000**, *122*, 1289− 1297. See also ref 7d. With regard to their system, the present observation points out the significance of the core geometry on the photophysical features of the conjugated rod assembly.

Table 2. Thermodynamic Data Associated with Dissolution as Extracted from the Analysis of the Solubility of the Molecular Rods (*n*R) and Crosses (*n*C) as a Function of Temperature in Cyclohexane (*n* = 1−3) (See Text)

molecule	$K°$(311 K)^a ± 5%	$\Delta_1 G°$(311 K) ± 5%^{a} (kJ mol^{-1})	$\Delta_1 H°$ ± 1^b (kJ mol^{-1})	$\Delta_1 S°$ ± 10^b (J K^{-1} mol^{-1})
1R	3.0 10^{-2}	9.1	12	5
2R	1.1 10^{-2}	11.6	35	75
3R	2.4 10^{-4}	21.7	44	70
1C	3.3 10^{-4}	20.7	11	−35
2C	6.2 10^{-5}	25.1	35	30
3C	3.7 10^{-5}	26.4	52	80

^{a} Solubility at 311 K (standard state: ideal solute at 1 M for the infinitely diluted solution). See Experimental Section. ^{b} Assumed to be constant in the range [290−330 K].

present study except methanol. In particular, the crosses **2C** and **3C** can be solubilized at concentrations as large as 98% (w/w) in good solvents such as dioxane! The corresponding solutions are optically homogeneous and do not scatter light. To quantitatively analyze the solubility in relation to molecular structure, a poorer solvent was more suitable, and cyclohexane was chosen. Table 2 reports the thermodynamic constants $K°$-(311 K) of the *n*C and of the *n*R species (*n* = 1, 2, 3) in cyclohexane at 311 K, so as the corresponding standard Gibbs free energy at 311 K $\Delta_1 G°$(311 K) associated to dissolution. In both *n*C and *n*R series, $K°$(311 K) is a decreasing function of the rod length. Nevertheless, the corresponding decrease is less pronounced in the *n*C series than in the *n*R one. The study of $K°$ in cyclohexane as a function of temperature was used to extract the standard enthalpy $\Delta_1 H°$ and the standard entropy $\Delta_1 S°$ upon assuming the latter to remain constant in the temperature range investigated.[19] $\Delta_1 H°$ and $\Delta_1 S°$ increase as a function of the rod length in both *n*C and *n*R series.

Thermodynamic Data Related to the Fusion Process. For the present purpose, it was interesting to collect the thermodynamic features associated with the fusion process for *n*C and

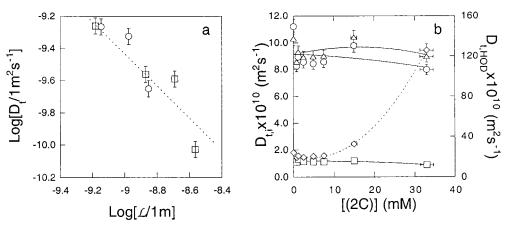(19) Lewis, G. N.; Brewer, L. *Thermodynamics*; McGraw-Hill: New York, Toronto, London, 1961.

Figure 3. (a) Dependence of the decimal logarithm of the translational self-diffusion coefficients of the **nR** (circles) and the **nC** (squares) molecules on their characteristic length $\mathscr{L}$ at 2 mM in dioxane-d_8 at 298 K ($n = 1-3$) (see text). The dotted straight line with a slope equal to -1 is displayed as a guideline for eyes. (b) Dependence of the translational self-diffusion coefficients of **2C** (squares), tetratrimethylsilane (circles), the residual protonated dioxane (triangles) and water (diamonds) as a function of the **2C** molar concentration in dioxane-d_8 at 298 K. The lines are given as guidelines for the eyes.

Table 3. Thermodynamic Data Extracted from DSC Measurements for the Molecular Rods (**nR**) and Crosses (**nC**) ($n = 1-3$)

molecule	$t_{transition}$ (K)	$\Delta_r H^* \pm 1$ (kJ mol^{-1})	$\Delta_r S^* \pm 10$ (J^{-1} K mol^{-1})^c
1R	360.5 ± 0.5^a	38	110
2R	389.5 ± 0.5^a	39	100
3R	477.5 ± 0.5^a	58	120
1C	482.5 ± 0.5^a	54	110
2C	363 ± 5^b	–	–
3C	390 ± 5^b	–	–

^{a} Melting point. ^{b} Shoulder. ^{c} $\Delta_r S^* = \Delta_r H^* / T_{Fusion}$.

Table 4. Translational Self-Diffusion Coefficients D_t Measured by ^{1}H NMR and Characteristic Lengths R_{sphere}, $\mathscr{L}_{rod}$, and $\mathscr{L}$ Resulting from Hydrodynamic Analysis and Molecular Modeling for the Molecular Rods **nR** and Crosses **nC** ($n = 1-3$)^a

molecule	D_t (10^{-10} m^2 s^{-1})	$R_{sphere} \pm 0.05$ (nm)^b	$\mathscr{L}_{rod} \pm 0.05$ (nm)^c	$\mathscr{L}$ (nm) $\pm 0.1^d$
1R	5.4 ± 0.2	0.30	1.5	1.4
2R	4.7 ± 0.2	0.35	2.1	2.0
3R	2.2 ± 0.1	0.75	8.00	2.8
1C	2.7 ± 0.1	0.60	–	0.9
2C	2.6 ± 0.1	0.65	–	1.7
3C	0.9 ± 0.1	1.80	–	2.1

^{a} Experimental conditions: 2 mM solutions in dioxane-d_8 at 298 K. See text and Experimental Section. ^{b} As extracted from eq 12 upon assuming the molecule to behave as a sphere; see Experimental Section. ^{c} As extracted from eq 13 upon assuming the molecule to behave as a rigid rod of diameter $\mathscr{D} = 0.4$ nm (average value based on consideration of the Hyperchem molecular models); see Experimental Section. ^{d} $\mathscr{L}$ corresponds either to the distance from the cross core to the arm extremity for **nC** crosses or to the length of the **nR** rods as evaluated from the Hyperchem molecular models.

nR. In fact, the ideal solubility of a pure solid compound in a solvent is related to its standard enthalpy of fusion and to its fusion temperature.[19,20] In addition, some information about the nature of condensed phases can be derived from calorimetry measurements. The results extracted from DSC records between 300 and 500 K are given in Table 3. The **nR** species exhibit a first-order transition ranging from 360.5 to 477.5 K that can be interpreted as a fusion. In contrast, only **1C** displays a melting point at 482.5 K among the investigated crosses. In fact, **2C** and **3C** thermograms only exhibit small reproducible shoulders at 363 and 390 K, respectively, that may be tentatively interpreted as glass transitions. As expected from solubility datas in cyclohexane, both fusion temperature T_f and standard enthalpy of fusion $\Delta_r H^*(T_f)$ are increasing functions of n in the **nR** series. In contrast, the corresponding standard entropies $\Delta_r S^*(T_f)$ remain rather similar.

NMR Investigation of nR and nC Solutions. nR and **nC** solutions in dioxane-d_8 have been examined by NMR to analyze the aggregation state and the freedom for molecular motions of the different solutes as a function of their concentration. In a first set of ^{1}H NMR translational self-diffusion experiments, the diffusion coefficients D_t of all the **nR** and **nC** species have been collected at 298 K at 2 mM in dioxane-d_8; at such a low concentration, monomeric species are anticipated so as to give reference values for the following series of NMR experiments. Figure 3a and Table 4 summarize the results. The measured diffusion coefficients are decreasing function of the characteristic molecular lengths $\mathscr{L}$ (rod length in the **nR** series and arm length in the **nC** series). More precisely, D_t roughly linearly depend on $1/\mathscr{L}$ in both series as suggested from Figure 3a. In a second

series of experiments, the structure of **2C** concentrated solutions in dioxane-d_8 has been more especially investigated to evaluate the significance of the cross shape on reducing the trend for crystallization or aggregation. ^{1}H NMR translational self-diffusion experiments were used to detect the possible formation of any **2C** aggregates upon increasing the solution concentration. Attention has been paid on the NMR line shape, on the signal integration and on the translational self-diffusion coefficient of **2C** in the 0.2−35 mM range. In fact, aggregation is expected to decrease at the same time the molecular correlation time and mobility. During the present study, the residual protonated dioxane and tetratrimethylsilane (TMS) were used as internal references. Indeed, both species are small enough to see their integration remaining essentially unaffected even in the presence of an intricated network such as pictured in Figure 1. In addition, the diffusion coefficients of the corresponding species could be used in principle to probe any percolation phenomenon associated to viscosity changes or excluded volumes. With regard to protonated dioxane and TMS, neither significant change of the **2C** NMR line shape nor anomaly of **2C** integration have been ever detected in the investigated range of concentrations (0.2−35 mM). To confirm this observation suggesting the absence of aggregates even at the largest concentrations, a magic angle spinning (MAS) ^{13}C NMR spectrum was recorded on the most **2C** concentrated sample. The corresponding sequence is

(20) Lemarchand, H.; Guyot, F.; Jousset, L.; Jullien, L. *Thermodynamique de la Chimie*; Hermann: Paris, 1999.
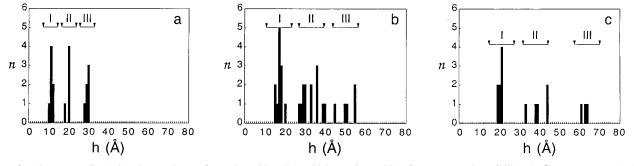
Figure 4. Histograms displaying the number n of samples with a given thickness h, resulting from evaporation of diluted n**C** DME: water 9:1 (v/v) solutions on mica surfaces as evaluated by multiple beam interferometry. (a) **1C**; (b) **2C**; (c) **3C**. I, II, and III respectively define the clusters that have been considered to correspond to films involving mono-, bi-, and trilayers. See text and Experimental Section.

known to reveal any species exhibiting structural features that forbid detection using liquid-state NMR.[21] The absence of any significant difference of integration ratios between the two NMR spectra recorded led to the first evidence that no large **2C** aggregates formed even at concentrations as high as 98% (w/w) in dioxane-d_8. Figure 3b displays the evolution of the diffusion coefficients obtained during the second series of ^{1}H NMR translational self-diffusion experiments. In the investigated concentration range, the self-diffusion coefficients of all the species but water remain essentially constant upon varying **2C** concentration in dioxane-d_8. In fact, the self-diffusion coefficient of water strongly increases at the largest **2C** concentrations.

Structure of Thin nC Films on Mica Surfaces. In view of their flatness, mica plates have been chosen to examine whether it was possible to obtain homogeneous thin films of the n**C** crosses on surfaces. In addition, multiple beam interferometry can be fruitfully used to determine the thickness of films deposited between two mica sheets at angström resolution.[5c] After preliminary investigation, 9:1 ethylene glycol dimethyl ether (DME):water (v/v) was selected as the n**C** organic solvent for deposition due to its good wetting properties toward mica. Eventually, 10 μM was chosen for n**C** concentrations to lead less than a unimolecular layer after solvent evaporation upon assuming the formation of a uniform film.[22] Under the present experimental conditions, evaporation of 5 μL of 10 μM n**C** solution in DME−water (9/1 (v/v)) deposited on mica did not give a homogeneous film at the scale of the whole spread drop. In particular, the fringe observation showed the presence of thick films in the zones corresponding to the drop rim.[23] In contrast, the observation of bumps in the fringes in the middle of the evaporated drop revealed the presence of very thin islands of diameter lying in the micrometer range. Figure 4, a−c, displays the histograms picturing the number of n**C** islands of a given thickness as measured by multiple beam interferometry. The major feature of these histograms is the existence of rather regularly spaced clusters ranging at multiples of molecular heights.

Discussion

Thermodynamic Analysis of the Solubility in Relation to Molecular Structure. A thermodynamic model has to be developed to examine the true significance of molecular shape on solubility. In fact, solubility is expected to be governed by both the geometry and the characteristic lengths of the considered molecule. Thus, it is necessary to appropriately normalize lengths to extract the role of molecular structure only. For the latter purpose, we assume in the present analysis (i) the molecules n**C** and n**R** to be strictly analogous in each series. Then the n**R** (respectively n**C**) molecules are only characterized by their length $\mathscr{L}$ (respectively the length $\mathscr{L}$ of the four arms grafted on the central node); (ii) the standard enthalpy associated to the dissolution process 1 to only depend on $\mathscr{L}$ in each series.[24] In the following, $\Delta_1 H°(T, \mathbf{M}, \text{length unit})$ and $\Delta_1 S°(T, \mathbf{M}, \text{length unit})$ are respectively defined as the common standard enthalpy and entropy changes associated to the dissolution process 1 per length unit in a given series n**M** ($\mathbf{M} = \mathbf{C}$ or $\mathbf{R}$). Upon assuming (i) and (ii), one obtains:

$$\Delta_1 H°(T, n\mathbf{M}) = i\mathscr{L}\Delta_1 H°(T, \mathbf{M}, \text{length unit}) \qquad (4)$$

with $i = 1$ when $\mathbf{M} = \mathbf{R}$, and $i = 4$ when $\mathbf{M} = \mathbf{C}$. Then, one easily derives:

$$\Delta_1 H°(T, n\mathbf{M}) = n\Delta_1 H°(T, \mathbf{1M}) \qquad (5)$$

Figure 5a displays the derived experimental relationship between $\Delta_1 H°(311\ \text{K}, n\mathbf{M})$ and n. Although being based on three points, satisfactory linear fits of the datas were obtained: $\Delta_1 H°(311\ \text{K}, n\mathbf{R})$ (kJ mol^{-1}) $= -8.6 + 20.5n$ and $\Delta_1 H°(311\ \text{K}, n\mathbf{C})$ (kJ mol^{-1}) $= -1.7 + 16.0n$. In contrast to the strict expectations from the relation 5, one notices in both cases the non-zero intercept with the y-axis so as the difference between

(21) Virlet, J. Line Narrowing Methods in Solids. In *Encyclopedia of Magnetic Resonance*; Grant, D. M., Harris, R. K., Eds,; Wiley: New York, 1996; p 2694. On a natural abundance carbon-13 sample, the use of MAS combined with high-power proton decoupling enables one to observe the signal due to any species in a solid or almost solid phase. A direct ^{13}C excitation has also been used instead of a cross polarization (CP)-MAS enhancement transfer to detect the molecules in solution.

(22) The latter estimate is obtained by considering the formation of a disc of 17 mm diameter on mica from evaporation of a 5 μL drop of 10 μM solution (see Experimental Section). Then the average surface per molecule is about 80 nm^2, whereas the evaluation from molecular models is 10 nm^2/molecule at the most (see Table 5).

(23) The present morphology probably results from mass and heat transfers occurring during solvent evaporation.

(24) Assumption (i) could be somehow questioned in view of the presence of the ethyl ester substituents on the terminal phenyl groups, and of the central node in the n**C** series. Nevertheless, it is expected to become satisfactory when n increases. Along the assumption (ii), the n**M** standard molar enthalpies in both liquid and solid phases, $h°(T, n\mathbf{M}, \text{solute})$ and $h°(T, n\mathbf{M}, \text{solid})$, are expected to only depend on $\mathscr{L}$ in each series ($\mathbf{M} = \mathbf{C}$ or $\mathbf{R}$). Such an assumption is natural for the former phase. For a short-range interaction such as van der Waals at this scale (see ref 5c), the solvent−solute interaction is governed by the surface contact scaling as $\mathscr{L}\mathscr{D}$ where $\mathscr{D}$ designates the rod diameter. In contrast, the same assumption could be questioned for the solid phase. In fact, it implies that the structure of the solid does not considerably evolve upon changing n within each series. The common elongated shape of the n**R** molecules together with the expected large compacity of their solid phase (the pure n**R** solids are crystals; vide supra) make the assumption reasonable in the n**R** series. In contrast, the same assumption could a priori appear more doubtfull for the n**C** molecules (see the differences of the DSC results in the n**C** series; vide supra) but will be ultimately validated by the experimental results (vide infra).
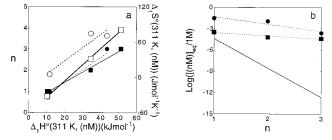
Figure 5. Relationships between thermodynamic datas associated to the dissolution process 1 for the $n\mathbf{M}$ molecules in cyclohexane at 311 K ($\mathbf{M} = \mathbf{R}$, circles; $\mathbf{M} = \mathbf{C}$, squares). (a) relationships between $\Delta_1 H°$-(311 K, $n\mathbf{M}$) and n (filled markers), and between $\Delta_1 S°(311\ K, n\mathbf{M})$ and $\Delta_1 H°(311\ K, n\mathbf{M})$ (empty markers). The thin and thick lines respectively picture the best linear fits of the experimental points $\Delta_1 H°$-(311 K, $n\mathbf{M}$)(n) and $\Delta_1 S°(311\ K, n\mathbf{M})[\Delta_1 H°(311\ K, n\mathbf{M})]$ ($\mathbf{M} = \mathbf{R}$, dotted line; $\mathbf{M} = \mathbf{C}$, solid line). Note that $\Delta_1 H°(311\ K, \mathbf{2C}) = \Delta_1 H°$-(311 K, $\mathbf{2R}$). (b) Evolution of the decimal logarithm of the $n\mathbf{M}$ solubilities in cyclohexane at 311 K. Markers: experimental points; dotted lines: best linear fits of the experimental points; solid line: $n\mathbf{Ref}$ expected behavior according to eq 10.

the slopes $sn\mathbf{M}$ of the $\Delta_1 H°(311\ K, n\mathbf{M})(n)$ linear fits, and $\Delta_1 H°(311\ K, \mathbf{1M})$ (see Table 2). In fact, end-groups (ethyl ester groups and central core in the $n\mathbf{C}$ series) probably weaken the van der Waals interaction involving the conjugated parts in the smallest terms of the series,[24] so as to introduce some curvature in the $\Delta_1 H°(311\ K, n\mathbf{M})(n)$ dependence. As anticipated by neglecting the negative term of second order when performing the linear fit, one thus coherently observes: (i) negative intercepts of the linear fits with the y-axis. Nevertheless, these intercepts can be considered as small (using the slope $sn\mathbf{M}$ of the $\Delta_1 H°$-(311 K, $n\mathbf{M}$)(n) for scaling: $8.6 \ll sn\mathbf{R} = 20.5$ in the $\mathbf{R}$ series and $1.7 \ll sn\mathbf{C} = 16.0$ in the $\mathbf{C}$ series); (ii) $sn\mathbf{R} > \Delta_1 H°(311\ K, \mathbf{1R})$ and $sn\mathbf{C} > \Delta_1 H°(311\ K, \mathbf{1C})$. Despite the latter small deviations, only the linear relation 5 was retained in the following to facilitate the subsequent calculations conceived to derive orders of magnitude. To progress further in the theoretical treatment of experimental datas, some extrathermodynamic relationship was sought for between the standard enthalpy and entropy changes associated to the dissolution process 1 per length unit in each series $n\mathbf{M}$ ($\mathbf{M} = \mathbf{C}$ or $\mathbf{R}$). Such relations are common in organic chemistry.[6b] Figure 5a does exhibit some reasonable trend for a linear relationship between $\Delta_1 S°(T, n\mathbf{M})$ and $\Delta_1 H°(T, n\mathbf{M})$ in each series. Introducing the slope $\beta(T, \mathbf{M})$ ($\beta(T, \mathbf{R}) = 2.3\ 10^{-3}\ \mathrm{K}^{-1}$ and $\beta(T, \mathbf{C}) = 2.8\ 10^{-3}\ \mathrm{K}^{-1}$), one writes:

$$\Delta_1 S°(T, n\mathbf{M}) - \Delta_1 S°(T, \mathbf{1M}) = \beta(T, \mathbf{M})[\Delta_1 H°(T, n\mathbf{M}) - \Delta_1 H°(T, \mathbf{1M})] \quad (6a)$$

or similarly:

$$\Delta_1 S°(T, \mathbf{M}, \text{length unit}) = \beta(T, \mathbf{M})\Delta_1 H°(T, \mathbf{M}, \text{length unit}) \quad (6b)$$

From eqs 5 and 6a, it is then possible to derive the dependence of the solubility $[n\mathbf{M}]_{eq}$ of the $n\mathbf{M}$ species on n:

$$\log([n\mathbf{M}]_{eq}) = n\log\{\alpha(T, \mathbf{1M})[\mathbf{1M}]_{eq}\} - \log\alpha(T, \mathbf{1M}) \quad (7)$$

where the parameter α defined as:

$$RT\log\{\alpha(T, \mathbf{1M})[\mathbf{1M}]_{eq}\} = [\beta(T, \mathbf{M})T - 1]\Delta_1 H°(T, \mathbf{1M}) \quad (8)$$

is introduced with R, the gas constant, and log the decimal logarithm, to facilitate the linear analysis when plotting log-$([n\mathbf{M}]_{eq})(n)$. Eventually it becomes now possible to extract the significance of the molecular geometry from the datas collected in the $n\mathbf{C}$ and $n\mathbf{R}$ series upon using the appropriate length normalization. For the present purpose, the rod $n\mathbf{Ref}$ of length $4\mathscr{L}$ is introduced as the reference compound for the cross $n\mathbf{C}$ with arm length $\mathscr{L}$. Thus, the corresponding standard enthalpy change associated to the dissolution process 1 and the $n\mathbf{Ref}$ solubility features are obtained from the preceding results derived in the $n\mathbf{R}$ series. Thus, one has:

$$\Delta_1 H°(T, n\mathbf{Ref}) = 4\Delta_1 H°(T, n\mathbf{R}) \quad (9)$$

$$\log([n\mathbf{Ref}]_{eq}) = 4n\log\{\alpha(T, \mathbf{1R})[\mathbf{1R}]_{eq}\} - \log\alpha(T, \mathbf{1R}) \quad (10)$$

The latter equations allow to interpret the evolution of the experimental solubilities displayed in Figure 5b. The linear dependence of $\log([n\mathbf{M}]_{eq})$ on n expected from eq 7 is satisfactorily verified in both $n\mathbf{M}$ series. Moreover, it can be used to directly extract $\alpha(T, \mathbf{1M})$ with more reliability than when using eqs 6a and 8, and the $\beta(T, \mathbf{1M})$ value derived from the analysis of the preceding extrathermodynamic relationship. Hence, one finds $\log\alpha(T, \mathbf{1R}) = 0.3$ and $\log\alpha(T, \mathbf{1C}) = 3.1$. The experimentally observed decrease of the $n\mathbf{M}$ solubility when n rises can also be interpreted from eqs 7 and 8. In fact, the $\beta(T, \mathbf{M})$ values derived from analysis of Figure 5a are such that $\{\alpha(T, \mathbf{1M})[\mathbf{1M}]_{eq}\} < 1$ around room temperature so as to make $[n\mathbf{M}]_{eq}$ a decreasing function of n from eq 7.

The comparison between the datas collected in the $n\mathbf{R}$ and the $n\mathbf{C}$ series is now performed. Equation 9 is first discussed in relation with Figure 5a showing that $\Delta_1 H°(T, n\mathbf{Ref}) \gg \Delta_1 H°$-$(T, n\mathbf{C}) \approx \Delta_1 H°(T, n\mathbf{R})$. Since $h°(T, n\mathbf{C}, \text{solute}) \approx h°(T, n\mathbf{Ref}, \text{solute})$ is anticipated,[25] one deduces $h°(T, n\mathbf{C}, \text{solid}) \gg h°(T, n\mathbf{Ref}, \text{solid})$ which suggests that molecular interactions are much stronger in the $n\mathbf{Ref}$ solid phase than in the $n\mathbf{C}$ one. Such an analysis is in line with the expectations based on molecular structures. In the solid state, the $n\mathbf{R}$ molecules are enough "compact" to give crystals whereas the more open structures of the largest crosses forbid crystal formation and lead to glasses such as pictured in Figure 1c. In the latter case, significant molecular interactions would only occur at the level of the few intermolecular contact points leading to low values of $h°(T, n\mathbf{C}, \text{solid})$. Sample observation, microanalyses and DSC results are in line with the latter conclusion. All of the $n\mathbf{R}$ species are crystalline, give correct microanalyses, and exhibit a melting point. In contrast, $\mathbf{2C}$ and $\mathbf{3C}$ samples are powders containing some residual solvent and do not exhibit any first-order transition in the DSC scans. Equation 10 is now addressed. Figure 5b compares the solubility of $n\mathbf{Ref}$ and $n\mathbf{C}$ at 311 K in cyclohexane. $[n\mathbf{C}]_{eq}$ always exceeds $[n\mathbf{Ref}]_{eq}$ by several orders of magnitude. In fact, $[n\mathbf{C}]_{eq}$ appears only poorly sensitive to n, whereas $[n\mathbf{Ref}]_{eq}$ is a decreasing function of n. Thus $\mathbf{3C}$ is already more than 10^8 times more soluble than $n\mathbf{Ref}$ in cyclohexane under ambient conditions, and the trend is anticipated to be more pronounced for larger n values! The latter observation is most conveniently analyzed in relation with eq

(25) As explained in ref 24, $h°(T, n\mathbf{M}, \text{solute})$ is reasonably expected to depend only on the characteristic length $\mathscr{L}$. In addition, $h°(T, n\mathbf{C}, \text{solute}, \text{length unit})$ is anticipated to marginally depend on the presence of the central node since the small cyclohexane molecules can easily access to the whole arm length. Thus, one can reasonably assume $h°(T, n\mathbf{C}, \text{solute}, \text{length unit}) \approx h°(T, n\mathbf{R}, \text{solute}, \text{length unit})$ so as to eventually write $h°(T, n\mathbf{C}, \text{solute}) \approx h°(T, n\mathbf{Ref}, \text{solute})$.

6b by noticing that $\beta(T, \mathbf{R}) < \beta(T, \mathbf{C})$; for the same standard entropy change associated to the dissolution process 1 per length unit, the corresponding standard enthalpy change is lower in the $n\mathbf{C}$ series than in the $n\mathbf{R}$ one. Hence, the favorable enthalpic term is not totally counterbalanced by an unfavorable entropic one in the $n\mathbf{C}$ series, and the crosses are comparatively much more soluble than the rods.

Thus, the analysis of thermodynamic datas confirms that a suitable molecular shape can considerably improve molecular solubility; decreasing the lattice energy of a solid phase is indeed an efficient strategy to promote dissolution, even in poor solvents such as cyclohexane.

Structure of Solutions of the $n\mathbf{C}$ Crosses. The analyses of the integration or line shape of the signals obtained during the ^{1}H NMR experiments showed that large $\mathbf{2C}$ aggregates did not form in dioxane-d_8, even at the highest concentration investigated (33 mM; 98% (w/w)). In addition, ^{1}H NMR translational self-diffusion experiments emphasized no significant evolution of the $\mathbf{2C}$ self-diffusion coefficient to take place in the concentration range 0.2–35 mM. To prove that the monomeric form was the major species present in $\mathbf{2C}$ solutions even at the largest concentrations, the experimental self-diffusion coefficients of the $n\mathbf{R}$ and $n\mathbf{C}$ molecules were analyzed with a hydrodynamic model. Upon assuming the molecules to behave as rigid bodies of given shapes in a continuous medium, Stokes–Einstein relations can be used to derive molecular dimensions from the self-diffusion coefficients and the solvent viscosity.[17] Empirical relations are available for the right cylinder geometry that is appropriate for describing the $n\mathbf{R}$ molecules (see Experimental Section). In contrast, no such relation seems to be available for tetrahedral stars. In a purpose of comparison, the crosses were consequently modeled as spheres since a simple relation is available for the latter geometry (see Experimental Section). Table 4 summarizes the results of the present hydrodynamic analysis for 2 mM solutions of $n\mathbf{R}$ and $n\mathbf{C}$. In both series of molecules, the agreement is satisfactory as demonstrated by (i) the experimentally observed linear dependence of D_t on $1/\mathscr{L}$ conforming to eqs 12 and 13; (ii) the comparison between the extracted characteristic lengths and the monomer dimensions.[26] In connection to the absence of change of the $\mathbf{2C}$ self-diffusion coefficient in the 0.2–35 mM concentration range, this analysis: (i) suggests that the solutions of crosses contain only monomeric species even at the largest concentrations. Such a conclusion is in line with the low trend for crystallization exhibited by the largest $n\mathbf{C}$ molecules; (ii) validates a posteriori the interpretation of the measured diffusion coefficients in the second series of NMR experiments. Indeed it was legitimate to analyze the latter at the molecular level without involving differently moving species in a regime of fast exchange.

In the second series of ^{1}H NMR translational self-diffusion experiments, the absence of evolution of the self-diffusion

---

(26) At a better level of analysis, one notices that the extracted length $\mathscr{L}_{\text{rod}}$ in the $n\mathbf{R}$ series is much too large for $\mathbf{3R}$, whereas it is much satisfactory for $\mathbf{1R}$ and $\mathbf{2R}$. This discrepancy is tentatively interpreted upon considering that the characteristic molecular length of $\mathbf{3R}$ cannot be neglected in front of the average intermolecular distance at 2 mM which lies around 0.9 nm. The solution cannot be anymore considered as diluted. Then two consequences are anticipated: (i) a possible drop of the self-diffusion coefficient due to collisions between $\mathbf{3R}$ molecules; (ii) some nematic order among the rodlike molecules leading to a dimensional restriction of the $\mathbf{3R}$ molecule translational motion. Under such conditions a data treatment based on free motion in three dimensions will underestimate the self-diffusion coefficient by a factor equal to $d/3$ where d represents the actual dimension in which molecular motion is restricted. The same analysis cannot be easily performed in the $n\mathbf{C}$ series. Nevertheless, the sphere model applies surprisingly rather well to describe the hydrodynamic of the crosses upon considering the similarity between the extracted radii and the arm lengths $\mathscr{L}$.

coefficients of all the species but water underlines that no major modification of molecular mobility occurs upon concentrating; the solution seems to remain in a diluted regime even at the 98% (w/w) concentration. To evaluate the latter result, the average distance $\langle r \rangle$ between two $\mathbf{2C}$ molecules was derived upon considering that the solute is distributed over a regular cubic lattice. At the 98% (w/w) concentration, $\langle r \rangle$ is about 3.6 nm which is only twice the length of the lateral $\mathbf{2C}$ arms (see Table 4). Under such conditions, the observation of a diluted regime may appear surprising for $\mathbf{2C}$ but probably reveals some intrisic geometrical feature of the open and anisotropic shape of the $\mathbf{2C}$ cross. The diffusion behavior of water in concentrated $\mathbf{2C}$ solutions is singular; its self-diffusion coefficient considerably increases at the largest concentrations. The solvent effect associated to the change of water environment at the largest $\mathbf{2C}$ concentrations cannot account for such a major increase. In fact, the viscosity of an aromatic solvent such as benzene or toluene is about half that of dioxane at room temperature. Thus a solvent effect only could increase the diffusion coefficient of water by a factor 2 at the most (see eq 12). In view of the value of the self-diffusion coefficient of water at low $\mathbf{2C}$ concentration which is in reasonable agreement with a monomeric state, no aggregate breaking can be invoked to explain the mobility rise of the water molecules. Upon considering hydrophobic forces, we tentatively propose the translational motion of the water molecules to be restricted in a percolated medium of low dimension in the $\mathbf{2C}$ network at the largest concentrations. Then the usual analysis based on a free motion occurring in three dimensions would lead to too large an apparent self-diffusion coefficient.

Thus ^{1}H NMR experiments emphasized that both monomeric states and translational degrees of freedom are essentially kept even in very concentrated solutions of crosses. From a practical point of view, the latter features are distinct advantages to obtain homogeneous thin films resulting from the spreading and the evaporation of solutions as it will be demonstrated in the next paragraph.

Structure of Thin Films Made of $n\mathbf{C}$ Crosses. To conclude on the structure of the films resulting from evaporation of diluted $n\mathbf{C}$ solutions on surfaces, two major issues have to be addressed from the interferometry experiments performed on films: (i) the presence of discrete clusters in the histograms obtained from data analysis of very thin $n\mathbf{C}$ films; (ii) the characteristic heights associated to the average values over each observed cluster (Figure 4).

The first observation is reminiscent of the oscillatory force that is observed when molecules with not too irregular shapes are confined between two hard walls.[5c] In fact, the high symmetry of the $n\mathbf{C}$ crosses is especially favorable to observe such a phenomenon; only the orientation making contact of three $n\mathbf{C}$ arm ends with the mica surface is expected at the same time (i) to minimize molecular height, (ii) to maximize $n\mathbf{C}$: mica interaction. By analogy with the explanation given for spherical molecules or linear alkanes, such a behavior may be reasonably interpreted as resulting from some periodical order whose repeat distance is closely related to the molecular size. An organized structure such as displayed in Figure 1b could be prone to exhibit such a feature. Then the presence of discrete clusters in Figure 4 could be considered as a clue supporting the theoretically predicted cubatic order at large $n\mathbf{C}$ concentrations.[8]

Along with the preceding interpretation, Table 5 and Figure 6 display the average film thicknesses $h(i)$ extracted from the histograms of Figure 4 by assuming the clusters as respectively

Table 5. Theoretical Molecular Height and Surface, and Experimental Thicknesses of Layers of the Molecular Crosses nC ($n = 1-3$) as Evaluated from Molecular Models and Interferometry Experiments

molecule	$h_{Th}(1) \pm 0.1$ (nm)[a]	$\mathscr{S}$ (nm^2 molecule^{-1})[b]	$h(1) \pm 0.1$ (nm)[c]	S_n (nm/layer)[d]
1C	1.2	2	1.1	0.9
2C	2.3	7	1.7	1.7
3C	2.8	10	2.0	2.1

[a] As evaluated with the Hyperchem software from $h_{Th} = 4\mathscr{L}/3$ where $\mathscr{L}$ represents the total length of the cross arm (see text). [b] As evaluated from $\mathscr{S} = 4 \cos(\pi/6) \sin^2(\theta/2)\mathscr{L}^2$ with $\theta = \text{Arccos}(-1/3)$. [c] As experimentally determined from the average position of the data cluster at the lowest values of heights. [d] Slope extracted from the linear fit of the $h(i)$ experimental data.
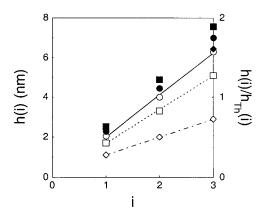

Figure 6. Evolution of the thickness $h(i)$ (empty markers) and of the ratio $h(i)/h_{Th}(i)$ (filled markers) of thin films measured by interferometry as a function of the number i of nC layers in the film. (Diamonds) **1C**; (squares) **2C**; (circles) **3C**. See text.

corresponding to mono-, bi, and trilayers of nC molecules ($i = 1-3$). Whatever the nC cross, the $h(i)$ values are linearly related to the number i of layers in the film. The latter observation probably indicates that the film density perpendicularly to the mica surface is reasonably independent of i for $i = 1-3$. In addition, both $h(1)$ and the slope S_n of the straight line $h(i)$ fitting as a function of i are significantly lower than the molecular height evaluated from molecular models. A first explanation could be some molecular entanglement taking place in the nC solid phase.[10] Nevertheless, it is hard to imagine this phenomenon to already occur for $i = 1$. Another explanation was envisaged from the favorable comparison between S_n and the arm lengths $\mathscr{L}$ of the nC crosses. To address the latter fact, we derived some orders of magnitude of energy to evaluate whether some molecular deformation could take place under the experimental conditions used during the interferometry experiments. In a first step, typical estimates of bending energies $W_b = k_\delta \theta \mathscr{N}_{\text{Avogadro}}$ associated to 10° bends were sought for. Upon assuming the bending motion to occur at the C−C≡C level, one obtains $W_b \approx 30$ kJ mol^{-1} whereas the corresponding value is about 100 kJ mol^{-1} if the bending takes place at the Arm−C−Arm central node of the tetraphenylmethane core.[27] In a second step, we evaluated the energies associated to possible van der Waals interactions occurring in the system with special emphasis on the dispersion interaction between a cross arm and the mica surface at contact. Hence, one obtains for the latter more than 100 kJ mol^{-1} for every members of the nC series by

taking 5 kJ mol^{-1} per carbon atom as a reasonable order of magnitude.[5c,28,29] The comparable estimates obtained in making these evaluations suggest that rather large molecular deformations could be envisaged to take place in the present system. In particular one could imagine the nC molecular tetrahedrons to tend to adopt the shape of a trigonal pyramid in order to maximize their interaction with the mica surfaces. In such a case, the molecular heights should be effectively close to the arm lengths as experimentally observed.

Consequently, the present investigation demonstrates that nC molecular crosses do lead to the formation of homogeneous thin films without building crystals at the micrometer scale. In contrast to nanoporous solids involving noncovalent interactions,[10] solvent removal does not promote the internal collapse of the present nanoporous structure. In addition, this study also suggests that some shape alteration of even the most "rigid" organic molecules could occur close to surfaces due van der Waals dispersive forces. In relation with the proposed strategy for favoring dissolution, the latter observation more generally emphasizes on the significance of the rigidity of the molecular motif that would be responsible of a low packing in the solid state. Indeed attractive forces are hudge at the molecular level so as to deform molecules to fill in any vacuum if they are not rigid enough.

Conclusions

The present study on rigid tetrahedral molecules considered as models of Onsager molecular crosses demonstrates that suitably designing molecular shape to avoid compact packing in the solid state is an efficient strategy to bypass crystallization and to promote dissolution of organic compounds in many solvents. Even in the absence of solubilizing substituents such as lateral chains or groups strongly interacting with the solvent, it has been possible to obtain homogeneous concentrated solution of monomeric rigid species that are traditionnally more prone to insolubility. In addition to the latter strong solubility improvement, an extremely concave molecular architecture was also shown to bring distinct advantages such as low viscosity and low trend for crystallization to obtain homogeneous pure nanoporous organic glasses after solvent removal even in ultrathin films. Despite this battery of attractive features, the present report also points on molecular rigidity as a limit that could be significant for several applications. In fact, even the traditionally envisioned most rigid organic backbones remain rather soft, and strong molecular deformation can be anticipated when such concave rigid molecules are located close to surfaces.

Experimental Section

Synthesis. General Procedures. Microanalyses were performed by the Service de Microanalyses de l′Université Pierre et Marie Curie (Paris). Melting points were determined with a Büchi 510 capillary apparatus or using DSC 7 Perkin-Elmer. ^{1}H and ^{13}C NMR spectra were

(27) Respectively using bending constants $k_\delta \approx 3 \times 10^{-19}$ N mrad^{-1} and $k_\delta \approx 10^{-18}$ N mrad^{-1}. See Herzberg, G. *Molecular Spectra and Molecular Structure II. Infrared and Raman Spectra of Polyatomic Molecules*; Krieger Publishing Company: Malabar, Florida, Original edition 1945: Reprint edition 1991.

(28) The present value is probably underestimated. In fact, the corresponding value is about 7 kJ mol^{-1} in the alkane series that exhibits a much less pronounced polarizability. See ref 5c.

(29) Other sources of van der Waals interaction are much less important. The energy W_{vdW} associated to the van der Waals attractive interaction between the mica sheets can be evaluated from the expression $W_{vdW} = -A/(12\pi h^2)$ where A designates the Hamaker constant of the system, and h, the distance between the two mica sheets.[5c] Taking $A = 10^{-20}$ J as a reasonable estimate for the Hamaker constant of a mica/organic medium/mica system,[5c] one obtains $W_{vdW} \approx 0.3$ mJm^{-2} for $h = 1$ nm and $W_{vdW} \approx 6$ μJm^{-2} for $h = 7$ nm. Thus, the pressure exerted by the mica surfaces on the thin films of nC can be neglected. Similarly, the direct attractive van der Waals interaction between cross arms in the solid state is expected to be rather small since molecular contact can occur only at a few sites due to the low compacity.

recorded at room temperature on a Bruker AM 200 SY, an Avance Bruker DRX 400 or an Avance Bruker DRX 600 spectrometers; chemical shifts are reported in ppm with protonated solvent as internal reference (^{1}H, CHCl$_3$ in CDCl$_3$ 7.27 ppm, protonated dioxane in dioxane-d_8 3.43 ppm; ^{13}C, [13]CDCl$_3$ in CDCl$_3$ 77.0 ppm); coupling constants J are given in Hz. Mass spectra (chemical ionization with NH$_3$ or FAB positive) were performed by the Service de Spectrométrie de Masse de l'ENS (Paris). Column chromatography was performed on silica gel 60 (0.040−0.063 mm) Merck. Analytical or preparative thin-layer chromatography (TLC) was conducted on Merck silica gel 60 F$_{254}$ precoated plates. Commercially available reagents were used as obtained.

4-(Trimethylsilylethynyl)aniline (2).[14] Trimethylsilylacetylene (3.9 mL, 27.4 mmol, 1.2 equiv) was added to a solution of 4-iodoaniline (**1**) (5.0 g, 23 mmol, 1 equiv) in deoxygenated distilled piperidine (20 mL) with tetrakis(triphenylphosphine)palladium(0) (658 mg, 0.57 mmol, 2.5 mol %) and copper iodide (43 mg, 0.23 mmol, 1 mol %) at 0 °C. After stirring for 3 h at room temperature, the reaction was quenched with a saturated aqueous solution of ammonium chloride, and dichloromethane was added. The aqueous layer was extracted twice with dichloromethane. The combined organic layers were washed with brine and dried over sodium sulfate. After evaporation of the solvent, the brown crude residue was purified by column chromatography on silica gel with dichloromethane/cyclohexane (70/30) as eluent to give **2** as a pale yellow solid (3.7 g, 85% yield): mp 93.5 °C (methanol, lit.[14] 95−96 °C); ^{1}H NMR (200 MHz, CDCl$_3$): $\delta = 7.28$ (apparent d, $J = 8.6$ Hz, 2H), 6.55 (apparent d, $J = 8.6$ Hz, 2H), 3.82 (bs, 2H), 0.27 (s, 9H); ^{13}C NMR (50 MHz, CDCl$_3$): $\delta = 146.7$, 133.1, 114.3, 112.1, 106.0, 91.2, 0.0.

1-Iodo-4-(trimethylsilylethynyl)benzene (3).[14] A solution of sodium nitrite (870 mg, 12.7 mmol, 1.2 equiv) in 2 mL of water was added to a solution of **2** (2.0 g, 10.6 mmol, 1 equiv) in 170 mL of hydrochloric acid (6 M) cooled below 5 °C. After stirring for 45 min at 0−5 °C, an ice-cold solution of potassium iodide (2.6 g, 16 mmol, 1.5 equiv) in 10 mL of water was poured dropwise, and 100 mL of dichloromethane was added. The resulting mixture was allowed to reach room temperature and was stirred for 4 h. The aqueous layer was extracted twice with dichloromethane, and the combined organic layers were washed with brine and dried over magnesium sulfate. After evaporation of the solvent, the crude residue was purified by column chromatography on silica gel with cyclohexane as eluent to give **3** as a pale yellow solid (2.1 g, 65% yield): mp 52.4 °C (methanol; lit.[12c] 56−58 °C); ^{1}H NMR (200 MHz, CDCl$_3$): $\delta = 7.63$ (apparent d, $J = 8.6$ Hz, 2H), 7.18 (apparent d, $J = 8.6$ Hz, 2H), 0.24 (s, 9H); ^{13}C NMR (50 MHz, CDCl$_3$): $\delta = 137.2$, 133.3, 122.6, 103.9, 95.7, 94.4, −0.2.

Diethyl-5-(amino)isophthaloate (5).[15] Thionyl chloride (12 mL, 165 mmol, 3 equiv) was added dropwise at 0 °C to a stirred solution of 5-(amino)isophthalic acid (**4**) (10 g, 55 mmol) in 100 mL of absolute ethanol. After stirring under reflux for 5 h, ethanol was distilled out. The crude residue was dissolved in ethyl acetate, and the solution was washed with a saturated aqueous solution of sodium bicarbonate. After drying over sodium sulfate, the solvent was evaporated to give the diester **5** as a white solid (11.6 g, 89%): mp 117.6 °C (ethanol, lit.[30] 118 °C); ^{1}H NMR (200 MHz, CDCl$_3$): $\delta = 8.06$ (t, $J = 1.4$ Hz, 1H), 7.53 (d, $J = 1.4$ Hz, 2H), 4.37 (q, $J = 7.1$ Hz, 4H), 3.82 (bs, 2H), 1.39 (t, $J = 7.1$ Hz, 6H); ^{13}C NMR (50 MHz, CDCl$_3$): $\delta = 166.0$, 146.5, 131.7, 120.5, 119.6, 61.3, 14.2.

Diethyl-5-(iodo)isophthaloate (6). The same procedure was used as for **3**. Sodium nitrite (3.5 g, 50 mmol, 1.2 equiv) in 30 mL of water; **5** (10 g, 42 mmol) in 11 mL of hydrochloric acid (2 M); potassium iodide (10.5 g, 63 mmol, 1.5 equiv) in 100 mL of water. Column chromatography on silica gel with dichloromethane as eluent to give **6** as a pale yellow solid (12.4 g, 85% yield): mp 76 °C (ethanol, lit.[31] 76 °C); ^{1}H NMR (200 MHz, CDCl$_3$): $\delta = 8.62$ (t, $J = 1.4$ Hz, 1H), 8.53 (d, $J = 1.4$ Hz, 2H), 4.40 (q, $J = 7.1$ Hz, 4H), 1.41 (t, $J = 7.1$ Hz, 6H); ^{13}C NMR (50 MHz, CDCl$_3$): $\delta = 164.2$, 142.1, 132.3, 129.6, 93.2, 31.6, 14.1.

Diethyl-5-(trimethylsilylethynyl)isophthaloate (1P).[12b] The same procedure was used as for **2**. Trimethylsilylacetylene (1.8 mL, 12.8

(30) Beyer, B. *J. Prakt. Chem.* **1882**, *25*, 465−517.

(31) Burton, H.; Kenner, J. *J. Chem. Soc.* **1923**, *123*, 1043−1045.

mmol, 1.2 equiv); **4** (3.7 g, 10.7 mmol, 1 equiv); tetrakis(triphenylphosphine)palladium(0) (308 mg, 0.27 mmol, 2.5 mol %); copper iodide (20 mg, 0.11 mmol, 1 mol %); piperidine (20 mL). Column chromatography on silica gel with dichloromethane as eluent to give **1P** as a pale yellow solid (3.0 g, 88% yield): mp 66.2 °C; ^{1}H NMR (200 MHz, CDCl$_3$): $\delta = 8.60$ (t, $J = 1.7$ Hz, 1H), 8.28 (d, $J = 1.7$ Hz, 2H), 4.40 (q, $J = 7.1$ Hz, 4H), 1.41 (t, $J = 7.1$ Hz, 6H), 0.27 (s, 9H); ^{13}C NMR (50 MHz, CDCl$_3$): $\delta = 164.9$, 136.5, 130.9, 130.0, 123.8, 102.7, 96.3, 61.3, 14.1, −0.4; anal. calcd for C$_{17}$H$_{22}$O$_4$Si (318.44): C 64.12, H 6.96; found: C 64.13, H 6.87.

Diethyl-5-(ethynyl)isophthaloate (1H). Cesium carbonate (3.4 g, 10 mmol, 1.1 equiv) was added to a solution of **1P** (3.0 g, 9.4 mmol, 1 equiv) dissolved in an ethanol/dichloromethane mixture (10 mL/10 mL). The solution was vigorously stirred at room temperature for 1 h. After removal of the solvents under reduced pressure, the residue was dissolved in a water/dichloromethane mixture. The aqueous layer was extracted twice with dichloromethane, and the combined organic layers were dried over magnesium sulfate. After solvent evaporation, the crude residue was purified by column chromatography on silica gel with dichloromethane as eluent to yield **1H** as pale yellow crystals (2.15 g; 93% yield): mp 90.5 °C; ^{1}H NMR (200 MHz, CDCl$_3$): $\delta = 8.60$ (t, $J = 1.6$ Hz, 1H), 8.28 (d, $J = 1.6$ Hz, 2H), 4.38 (q, $J = 7.1$ Hz, 4H), 3.18 (s, 1H), 1.39 (t, $J = 7.1$ Hz, 6H); ^{13}C NMR (50 MHz, CDCl$_3$): $\delta = 164.8$, 136.7, 131.1, 130.4, 122.8, 81.5, 78.9, 61.4, 14.1; anal. calcd for C$_{14}$H$_{14}$O$_4$ (246.26): C 68.28, H 5.73; found: C 68.16, H 5.72.

Diethyl-5-[(4-[trimethylsilylethynyl]phenyl)ethynyl]-isophthaloate (2P). The same procedure was used as for **2** except that copper iodide was added at last. Copper iodide (10 mg, 0.05 mmol, 1 mol %); **1H** (1.3 g, 5.3 mmol, 1 equiv); **3** (1.6 g, 5.3 mmol, 1 equiv); tetrakis(triphenylphosphine)palladium(0) (122 mg, 0.1 mmol, 2 mol %); piperidine (20 mL). Column chromatography on silica gel with dichloromethane as eluent to give **2P** as a pale yellow solid (1.94 g, 88% yield): mp 74.2 °C (ethanol); ^{1}H NMR (200 MHz, CDCl$_3$): $\delta = 8.60$ (t, $J = 1.7$ Hz, 1H), 8.28 (d, $J = 1.7$ Hz, 2H), 7.47 (s, 4H), 4.42 (q, $J = 7.1$ Hz, 4H), 1.42 (t, $J = 7.1$ Hz, 6H), 0.26 (s, 9H); ^{13}C NMR (50 MHz, CDCl$_3$): $\delta = 164.9$, 136.2, 131.8, 131.4, 131.1, 130.0, 123.8, 123.4, 122.4, 104.3, 96.5, 90.5, 89.1, 61.4, 14.1, −0.3; anal. calcd for C$_{25}$H$_{26}$O$_4$Si (418.56): C 71.74, H 6.26; found C 71.82, H 6.44.

Diethyl-5-[(4-ethynylphenyl)ethynyl]isophthaloate (2H). The same procedure was used as for **1H**. **2P** (1.90 g, 4.54 mmol); cesium carbonate (1.63 g, 5 mmol, 1.1 equiv); ethanol/dichloromethane (1/1; 10 mL). Column chromatography on silica gel with dichloromethane as eluent to yield **2H** as pale yellow crystals (1.35 g; 87% yield): mp 87.8 °C; ^{1}H NMR (200 MHz, CDCl$_3$): $\delta = 8.61$ (t, $J = 1.7$ Hz, 1H), 8.33 (d, $J = 1.7$ Hz, 2H), 7.48 (s, 4H), 4.41 (q, $J = 7.1$ Hz, 4H), 3.20 (s, 1H), 1.42 (t, $J = 7.1$ Hz, 6H); ^{13}C NMR (50 MHz, CDCl$_3$): $\delta = 164.9$, 136.1, 131.9, 131.4, 131.1, 130.0, 123.7, 122.7, 122.3, 90.3, 89.2, 82.9, 79.1, 61.4, 14.1; anal. calcd for C$_{22}$H$_{18}$O$_4$ (346.38): C 76.29, H 5.24; found: C 76.21, H 5.32.

Diethyl-5-[(4-[(4-[trimethylsilylethynyl]phenyl)ethynyl]phenyl)-ethynyl]isophthaloate (3P). The same procedure was used as for **2P**. **2H** (1.1 g, 3.15 mmol); **3** (1.0 g, 3.15 mmol); tetrakis(triphenylphosphine)palladium(0) (73 mg, 0.06 mmol, 2 mol %); copper iodide (9 mg, 0.05 mmol, 1.5 mol %); piperidine (12 mL). Column chromatography on silica gel with dichloromethane/cyclohexane: 9/1 as eluent to give **3P** as pale yellow crystals (1.57 g; 96% yield): MS (CI, NH$_3$); m/z 535.0 (calcd av mass for C$_{33}$H$_{30}$O$_4$Si + NH$_3$: 535.71), 519.0 (calcd av mass for C$_{33}$H$_{30}$O$_4$Si: 518.6); mp 142 °C (*i*PrOH); ^{1}H NMR (200 MHz, CDCl$_3$): $\delta = 8.64$ (t, $J = 1.6$ Hz, 1H), 8.36 (d, $J = 1.6$ Hz, 2H), 7.53 (s, 4H), 7.46 (s, 4H), 4.44 (q, $J = 7.1$ Hz, 4H), 1.44 (t, $J = 7.1$ Hz, 6H), 0.26 (s, 9H); ^{13}C NMR (50 MHz, CDCl$_3$): $\delta = 165.2$, 136.4, 132.0, 131.8, 131.7, 131.5, 131.4, 130.2, 124.0, 123.5, 123.3, 123.0, 122.6, 104.6, 96.6, 91.2, 90.9, 90.8, 89.4, 61.7, 14.4, −0.1; anal. calcd for [90% C$_{33}$H$_{30}$O$_4$Si (518.6), 10% *i*PrOH]: C 75.53, H 5.93; found: C 75.31; H 5.80.

Diethyl-5-[(4-[(4-ethynylphenyl)ethynyl]phenyl)ethynyl]-isophthaloate (3H). The same procedure was used as for **1H**. **3P** (1.5 g, 2.9 mmol); cesium carbonate (1.1 g 3.4 mmol, 1.1 equiv); ethanol/dichloromethane (1/2; 15 mL). Column chromatography on silica gel with dichloromethane as eluent to give **3H** as pale yellow crystals (0.8 g; 61% yield): MS (CI, NH$_3$); m/z 464.0 (calcd av mass for C$_{30}$H$_{22}$O$_4$

+ NH$_3$: 463.5), 447.0 (calcd av mass for C$_{30}$H$_{22}$O$_4$: 446.5); mp 166 °C (dioxane/ethanol); ^{1}H NMR (200 MHz, CDCl$_3$): $\delta = 8.64$ (t, $J = 1.6$ Hz, 1H), 8.36 (d, $J = 1.6$ Hz, 2H), 7.54 (s, 4H), 7.49 (s, 4H), 4.44 (q, $J = 7.1$ Hz, 4H), 3.20 (s, 1H), 1.44 (t, $J = 7.1$ Hz, 6H); ^{13}C NMR (50 MHz, CDCl$_3$): $\delta = 165.2$, 136.4, 132.2, 131.8, 131.7, 131.5, 131.4, 130.2, 124.0, 123.5, 123.4, 122.6, 122.2, 91.0, 90.9, 90.8, 89.5, 83.2, 79.2, 61.7, 14.4; anal. calcd for C$_{30}$H$_{22}$O$_4$ (446.50): C 80.69, H 4.96; found: C, 80.09; H, 5.01.

Tetrakis[4-(iodo)phenyl]methane (8).[13b] A suspension of tetraphenylmethane (2.5 g, 5.5 mmol), bis(trifluoroacetoxy)iodobenzene (5.9 g, 13.7 mmol, 2.5 equiv), and iodine (4.2 g, 16.5 mmol, 3 equiv) in 35 mL of carbon tetrachloride was stirred at reflux for 16 h. After cooling at 40−35 °C, the suspension was filtered, and the solid residue was washed twice with 10 mL of dichloromethane. After drying, **8** was obtained as a pink powder (2.7 g; 60% yield): MS (CI, NH$_3$); m/z 824.0 (calcd av mass for C$_{25}$H$_{16}$I$_4$: 824.0); ^{1}H NMR (200 MHz, CDCl$_3$): $\delta = 7.60$ (apparent d, $J = 8.7$ Hz, 2H), 6.89 (apparent d, $J = 8.7$ Hz, 2H).

Tetrakis[4-(diethyl-5-[ethynyl]isophthaloate)phenyl]methane (1C). The same procedure was used as for **2P**. **8** (160 mg, 0.19 mmol, 1 equiv); **1H** (224 mg, 0.9 mmol, 4.8 equiv); tetrakis(triphenylphosphine)-palladium(0) (22 mg, 0.02 mmol, 10 mol %); copper iodide (2 mg, 0.01 mmol, 5 mol %); piperidine/tetrahydrofuran (4/1; 5 mL). Column chromatography on silica gel with dichloromethane as eluent to give **1C** as white crystals (200 mg, 82% yield); MS (CI, NH$_3$); m/z 1314.4 (calcd av mass for C$_{81}$H$_{68}$O$_{16}$ + NH$_3$: 1314.4); mp 209.1 °C (ethanol); ^{1}H NMR (200 MHz, CDCl$_3$): $\delta = 8.63$ (t, $J = 1.6$ Hz, 1H), 8.36 (d, $J = 1.6$ Hz, 2H), 7.50 (apparent d, $J = 8.2$ Hz, 2H), 7.25 (apparent d, $J = 8.2$ Hz, 2H), 4.43 (q, $J = 7.1$ Hz, 4H), 1.43 (t, $J = 7.1$ Hz, 6H); ^{1}H NMR (600 MHz, dioxane-d_8): $\delta = 8.54$ (t, $J = 1.7$ Hz, 1H), 8.35 (d, $J = 1.7$ Hz, 2H), 7.58−7.57 (dd, $J_{ortho} = 8.5$ Hz, $J_{meta} = 1.8$ Hz, 2H), 7.37−7.36 (dd, $J_{ortho} = 8.5$ Hz, $J_{meta} = 1.8$ Hz, 2H), 4.41 (q, $J = 7.1$ Hz, 4H), 1.41 (t, $J = 7.1$ Hz, 6H); ^{13}C NMR (50 MHz, CDCl$_3$): $\delta = 165.1$, 146.2, 136.3, 131.3, 131.2, 130.8, 130.0, 124.0, 120.7, 90.6, 87.9, 64.9, 61.5, 14.2; anal. calcd for C$_{81}$H$_{68}$O$_{16}$ (1297.42): C 74.98, H 5.28; found C 75.09, H 5.26.

Tetrakis[4-(diethyl-5-[(4-[ethynyl]phenyl)ethynyl]isophthaloate)-phenyl]methane (2C). The same procedure was used as for **2P**. **8** (160 mg, 0.19 mmol, 1 equiv); **2H** (315 mg, 0.9 mmol, 4.8 equiv), tetrakis-(triphenylphosphine)palladium(0) (22 mg, 0.02 mmol, 10 mol %); copper iodide (2 mg, 0.01 mmol, 5 mol %); piperidine/tetrahydrofuran (4/1; 5 mL). Column chromatography on silica gel with dichloromethane as eluent to yield **2C** as a pale yellow powder (260 mg; 81% yield). The sample for DSC was precipitated from dioxane/*i*PrOH: MS (FAB, TFA); m/z 1697.7 (calcd av mass for C$_{113}$H$_{84}$O$_{16}$: 1697.8); ^{1}H NMR (200 MHz, CDCl$_3$): $\delta = 8.65$ (t, $J = 1.6$ Hz, 1H), 8.37 (d, $J = 1.6$ Hz, 2H), 7.54 (s, 4H), 7.49 (apparent d, $J = 8.4$ Hz, 2H), 7.24 (apparent d, $J = 8.4$ Hz, 2H), 4.44 (q, $J = 7.1$ Hz, 4H), 1.44 (t, $J = 7.1$ Hz, 6H); ^{1}H NMR (600 MHz, dioxane-d_8): $\delta = 8.56$ (t, $J = 1.7$ Hz, 1H), 8.38 (d, $J = 1.7$ Hz, 2H), 7.65 (apparent d, $J = 8.3$ Hz, 2H), 7.60 (apparent d, $J = 8.3$ Hz, 2H), 7.52 (apparent d, $J = 8.4$ Hz, 2H), 7.34 (apparent d, $J = 8.4$ Hz, 2H), 4.42 (q, $J = 7.1$ Hz, 4H), 1.41 (t, $J = 7.1$ Hz, 6H); ^{13}C NMR (100 MHz, CDCl$_3$): $\delta = 165.1$, 146.0, 136.3, 131.6, 131.6, 131.2, 131.1, 130.8, 130.1, 123.9, 123.5, 122.3, 121.0, 91.0, 90.7, 89.4, 89.2, 64.9, 61.6, 14.2; anal. calcd for [1.00 mol of C$_{113}$H$_{84}$O$_{16}$ (1697.8), 0.60 mol of dioxane]: C 77.81, H 5.11; found: C 77.84, H 5.02.

Tetrakis[4-(diethyl-5-[4-(4-[ethynyl]phenyl)ethyny]phenyl)ethynyl]-isophthaloate) phenyl]methane (3C). The same procedure was used as for **2P**. (**8**) (160 mg, 0.19 mmol, 1 equiv); **3H** (405 mg, 0.9 mmol, 4.8 equiv); tetrakis(triphenylphosphine)palladium(0) (22 mg, 0.02 mmol, 10 mol %); copper iodide (2 mg, 0.01 mmol, 5 mol %); piperidine/tetrahydrofuran (4/1; 5 mL). Column chromatography on silica gel with dichloromethane to give **3C** as a pale yellow powder (374 mg; 94% yield): MS (FAB, NBA); m/z 2097.8 (calcd av mass for C$_{145}$H$_{100}$O$_{16}$: 2098.3); ^{1}H NMR (400 MHz, CDCl$_3$): $\delta = 8.64$ (t, $J = 1.5$ Hz, 1H), 8.36 (d, $J = 1.5$ Hz, 2H), 7.54 (s, 4H), 7.52 (s, 4H), 7.47 (apparent d, $J = 8.4$ Hz, 2H), 7.23 (apparent d, $J = 8.4$ Hz, 2H), 4.43 (q, $J = 7.1$ Hz, 4H), 1.44 (t, $J = 7.1$ Hz, 6H); ^{13}C NMR (100 MHz, CDCl$_3$): $\delta = 165.1$, 146.0, 136.3, 131.6, 131.5, 131.5, 131.2, 131.1, 130.8, 130.1, 123.9, 123.3, 123.2, 122.7, 122.4, 121.1, 91.2, 90.9, 90.8, 90.7, 89.5,

89.3, 64.8, 61.5, 14.2; anal. calcd for [1.00 mol of C$_{145}$H$_{100}$O$_{16}$ (2098.39), 0.22 mol of dioxane]: C 82.33, H 4.84; found: C 82.31, H 4.78.

Diethyl-5-[(phenyl)ethynyl)]isophthaloate (1R). The same procedure was used as for **2P**. ^{1}H (183 mg, 0.74 mmol); (**9**) (227 mg, 1.1 mmol, 1.5 equiv); tetrakis(triphenylphosphine)palladium(0) (43 mg, 0.04 mmol, 5 mol %); copper iodide (3 mg, 0.02 mmol, 2 mol %); piperidine (3 mL). Column chromatography on silica gel with dichloromethane as eluent to give **1R** as white crystals (227 mg, 95% yield): MS (CI, NH$_3$); m/z 322.99 (calcd av mass for C$_{20}$H$_{18}$O$_4$: 322.36); mp 87.3 °C (ethanol); ^{1}H NMR (200 MHz, CDCl$_3$): $\delta = 8.64$ (t, $J = 1.7$ Hz, 1H), 8.37 (d, $J = 1.7$ Hz, 2H), 7.62−7.57 (m, 2H), 7.42−7.38 (m, 3H), 4.43 (q, $J = 7.1$ Hz, 4H), 1.43 (t, $J = 7.1$ Hz, 6H); ^{13}C NMR (50 MHz, CDCl$_3$): $\delta = 164.8$, 136.0, 131.5, 131.0, 129.7, 128.6, 128.2, 124.0, 122.3, 90.9, 87.3, 61.3, 14.1; anal. calcd for C$_{20}$H$_{18}$O$_4$ (322.36): C 74.52, H 5.63; found: C 74.55, H 5.82.

Diethyl-5-[4-[(phenyl)ethynyl]phenyl]ethynyl]isophthaloate (2R). The same procedure was used as for **2P**. **2H** (197 mg, 0.57 mmol); (**9**) (174 mg, 0.85 mmol, 1.5 equiv); tetrakis(triphenylphosphine)palladium-(0) (33 mg, 0.03 mmol, 5 mol %); copper iodide (2 mg, 0.01 mmol, 2 mol %); piperidine (3 mL). Column chromatography on silica gel with dichloromethane as eluent to give **2R** as white crystals (220 mg, 91% yield): MS (CI, NH$_3$); m/z 422.0 (calcd av mass for C$_{28}$H$_{22}$O$_4$: 422.4); mp 116.3 °C (ethanol); ^{1}H NMR (200 MHz, CDCl$_3$): $\delta = 8.64$ (t, $J = 1.7$ Hz, 1H), 8.37 (d, $J = 1.7$ Hz, 2H), 7.57−7.53 (m, 6H), 7.40−7.35 (m, 3H), 4.42 (q, $J = 7.1$ Hz, 4H), 1.44 (t, $J = 7.1$ Hz, 6H); ^{13}C NMR (50 MHz, CDCl$_3$): $\delta = 165.1$, 136.3, 131.7, 131.6, 131.4, 130.2, 128.5, 128.4, 124.0, 123.8, 123.0, 122.3, 91.6, 90.8, 89.2, 89.0, 87.3, 61.6, 14.3; anal. calcd for C$_{28}$H$_{22}$O$_4$ (422.48): C 79.60, H 5.25, found: C 79.65, H 5.12.

Diethyl-5-[[4-[(4-[(phenyl)ethynyl]phenyl)ethynyl)phenyl]ethynyl]-isophthaloate (3R). The same procedure was used as for **2P**. **3H** (165 mg, 0.37 mmol); (**9**) (112 mg, 0.55 mmol, 1.5 equiv); tetrakis-(triphenylphosphine)palladium(0) (22 mg, 0.02 mmol, 5 mol %); copper iodide (1.5 mg, 0.01 mmol, 2 mol %); piperidine (2 mL). Column chromatography on silica gel with dichloromethane as eluent to give **3R** as a white powder (170 mg, 88% yield): MS (CI, NH$_3$); m/z 540.0 (calcd av mass for C$_{36}$H$_{26}$O$_4$ + NH$_3$: 539.6); mp 204.5 °C (ethanol/tetrahydrofuran); ^{1}H NMR (250 MHz, CDCl$_3$): $\delta = 8.65$ (t, $J = 1.6$ Hz, 1H), 8.37 (d, $J = 1.6$ Hz, 2H), 7.57−7.36 (m, 13H), 4.44 (q, $J = 7.1$ Hz, 4H), 1.44 (t, $J = 7.1$ Hz, 6H); ^{13}C NMR (100 MHz, CDCl$_3$): $\delta = 165.1$, 136.3, 131.6, 131.6, 131.5, 131.2, 130.1, 128.5, 128.3, 123.9, 123.4, 123.3, 122.9, 122.6, 122.4, 91.4, 91.2, 90.7, 90.7, 89.3, 89.0, 61.6, 14.3; anal. calcd for C$_{36}$H$_{26}$O$_4$ (522.60): C 82.74, H 5.01, found: C 82.62; H 5.21.

UV/Vis Spectroscopic Measurements. All experiments were performed at 298 K in spectroscopic grade methylene chloride. The UV/Vis absorption spectra were recorded on a Kontron Uvikon-930 spectrophotometer. Corrected fluorescence spectra were obtained with a Photon Technology International LPS 220 spectrofluorometer. Solutions for fluorescence measurements were adjusted to a specific concentration so that the maximum absorbance was ≤0.15 at the excitation wavelength. The overall fluorescence quantum yields of **nR** and **nC** were calculated from the relation:[32]

$$\Phi_u = \Phi_s \frac{A(\lambda)_s F_u n_u^2}{A(\lambda)_u F_s n_s^2} \tag{11}$$

where the subscripts s and u indicate the standard and unknown sample, $A(\lambda)$ corresponds to the absorbance of the solution at the excitation wavelength λ, F is the integrated emission spectrum, and n is the refractive index for the solvent carrying the unknown and the standard. The standard fluorophore for solution measurements was quinine sulfate in 0.1 M H$_2$SO$_4$ with $\Phi_s = 0.50$.[32]

Solubility Measurements. Enough of each compound **nM** (**M** = **R** or **C**) (1−10 mg) was added to 1 mL of analytical grade cyclohexane to keep some solid remaining in equilibrium with the solution in the whole temperature range investigated. After centrifugation and temperature reequilibration, an aliquot of 25 μL of supernatant was poured

(32) Demas, J. N.; Crosby, G. A. *J. Phys. Chem.* **1971**, *75*, 991−1024.

into 5 mL of dichloromethane. Then the corresponding solution was used for determining the saturated concentration in nM, $[n\text{M}]_{\text{eq},T}$, from UV absorption experiments. Eventually the thermodynamic constant $K°(T)$ associated with the dissolution process at T was evaluated from $K°(T) = [n\text{M}]_{\text{eq},T}/\text{C}°$ with $\text{C}° = 1$ mol L^{-1}).

DSC Experiments. Differential scanning calorimetry experiments were carried out using a DSC 7 Perkin-Elmer. The following procedure was applied for the n**R** and n**C** compounds (1−2 mg samples): first heating cycle (20−230 °C; 5 °C/min but 20 °C/min for **2C** and **3C**), cooling cycle (20−230 °C; 5 °C/min but 20 °C/min for **2C** and **3C**); second heating cycle (20−230 °C; 5 °C/min but 20 °C/min for **2C** and **3C**). TLC using reference compounds n**R** and n**C** was used to check that no degradation occurred during the DSC experiments.

NMR Studies. The measurements of translational diffusion coefficients were carried out on an Avance Bruker DRX 600 spectrometer equipped with a TBI probe with three orthogonal pulsed field gradients (PFG). The pulse sequence used was a double stimulated echo (DSTE) which suppresses the effects of fluid velocity (convection).[33] Eddy current effects were minimized using sine shaped PFG and introducing a longitudinal eddy current delay (LED) of 5 ms before acquisition. The total diffusion delay length was 200 ms. Encoding PFG lengths were of 2 ms for all experiments. Their maximum amplitudes were varied from 1.1 G·cm^{-1} to 52.9 G·cm^{-1} in 32 steps. Each experiment was acquired with 32 transients, except for **1R**, **2R**, and **1C** where eight transients led to good enough signal-to-noise ratios. Two dimension diffusion-ordered spectroscopy (DOSY) spectra were obtained after monoexponential inverse Laplace transformation and diffusion coefficients were measured, corresponding to the maximum intensity of the projection onto the diffusion axis (see Figure 2S). Additional peaks in the diffusion dimension were observed for each nucleus in each molecule. They arise from artifacts of the monoexponential inverse Laplace transform. In fact, the decrease of the intensity as a function of the squared gradient strength is not perfectly exponential.[34] Moreover, a biexponential inverse Laplace transform modifies the measured diffusion coefficient by less than 2%, so that the error introduced by these artifacts may be neglected.

Interferometry Experiments. Five microliters of 10 μM n**C** solution in DME-water (9/1 (v/v)) were spread on the clean side of a 2−5 μm-thin mica sheet silvered on the other side (transmittivity about 1% in green visible light) to yield discoidal films typically lying in 16−19 mm for the diameter. After evaporation in a vacuum for 30 min, a similar second piece of mica was put on. Collimated white light was

sent with normal incidence on the resulting interferometer. The transmitted beam collected with a lens consists of fringes of equal chromatic order (FECO) arising from constructive interference of the light reflected at the various interfaces of the interferometer.[5c] After analysis with a calibrated spectroscope, the FECO wavelengths independently provide both the film thickness at 0.1 nm accuracy and its refractive index. Upon scanning on a line by steps equal to 2 μm, one obtains interferometric pictures of the film cross section at a 4 μm lateral resolution. Under the present conditions, solvent evaporation produced islandlike homogeneous zones (characteristic size: at least several micrometers). At least 10 islands from each film were used to evaluate its thickness.

Derivation of Molecular Characteristic Lengths from Hydrodynamic Analysis of the Diffusion Coefficients D_t. Under considering the medium as a continuum and assuming stick boundary conditions to apply in the present case,[17] the following expressions were used to derive molecular characteristic lengths from the diffusion coefficients:

$$\text{Body assimilated to a sphere } D_t^{\text{sphere}} = \frac{kT}{6\pi\eta R_{\text{sphere}}} \quad (12)$$

where k is the Boltzmann constant, T the absolute temperature, η the medium viscosity and R_{sphere} the sphere radius.

Body Assimilated to a right Circular Cylinder (Length $\mathscr{L}_{\text{rod}}$, Diameter D). A semiempirical formula is available in the range $2 \leq p = \mathscr{L}_{\text{rod}}/\mathscr{D} \leq 30$.[35]

$$D_t = \frac{kT(\ln p + \nu)}{3\pi\eta\mathscr{L}_{rod}} \quad \text{with } \nu = 0.312 + 0.565/p - 0.100/p^2 \quad (13)$$

For the calculations, the viscosity of dioxane − d_8 was taken equal to 1.295 10^{-3} Pas at 298 K.[36]

Supporting Information Available: Additional figures (PDF). This material is available free of charge via the Internet at http://pubs.acs.org.

JA010019H

(33) Jerschow, A.; Muller, N. *J. Magn. Reson.* **1997**, *125*, 372−375.

(34) Johnson, C. S. *Prog. Nucl.Magn. Reson. Spectrosc.* **1999**, *34*, 203−256.

(35) Tirado, M. M.; Martinez, C. L.; Garcia De La Torre, J. *J. Chem. Phys.* **1984**, *81*, 2047−2052.

(36) Holz, M.; Mao, X.-A.; Seiferling, D.; Sacco, A. *J. Chem. Phys.* **1996**, *104*, 669−679.